
EAZY: Eliminating Hallucinations in LVLMs by Zeroing out Hallucinatory Image Tokens

Liwei Che

lc1279@cs.rutgers.edu

Tony Qingze Liu

ql236@scarletmail.rutgers.edu

Jing Jia

jing.jia@rutgers.edu

Weiyi Qin

wq50@cs.rutgers.edu

Ruixiang Tang

ruixiang.tang@rutgers.edu

Vladimir Pavlovic

vladimir@cs.rutgers.edu

Rutgers University

New Brunswick, NJ 08901

Abstract

Despite their remarkable potential, Large Vision-Language Models (LVLMs) still face challenges with object hallucination, a problem where their generated outputs mistakenly incorporate objects that do not actually exist. Although most works focus on addressing this issue within the language-model backbone, our work shifts the focus to the image input source, investigating how specific image tokens contribute to hallucinations. Our analysis reveals a striking finding: a small subset of image tokens with high attention scores are the primary drivers of object hallucination. By removing these hallucinatory image tokens (only 1.5% of all image tokens), the issue can be effectively mitigated. This finding holds consistently across different models and datasets. Building on this insight, we introduce EAZY, a novel, training-free method that automatically identifies and Eliminate hAllucinations by Zeroing out hallucinatorY image tokens. We utilize EAZY for unsupervised object hallucination detection, achieving 15% improvement compared to previous methods. Additionally, EAZY demonstrates remarkable effectiveness in mitigating hallucinations while preserving model utility and seamlessly adapting to various LVLM architectures.

1 Introduction

Large Vision-Language Models (LVLMs) [Liu et al., 2024c,a, Chiang et al., 2023] have achieved remarkable advancements, seamlessly integrating visual recognition and language understanding to produce outputs that are both coherent and contextually aligned. Despite these successes, LVLMs face a critical challenge from hallucination [Liu et al., 2024d]. Hallucination in LVLMs manifests as generating incorrect responses that either contradict the provided image input or deviate from user instructions. This problem not only compromises LVLMs reliability but also limits their broader applicability in real-world scenarios. Among the various forms of hallucination, object hallucination (OH) [Rohrbach et al., 2018] is particularly prevalent. This occurs when LVLMs either misidentify objects or incorrectly perceive hallucinatory objects (HO) as being present in an image. Addressing this issue is essential to enhance the accuracy and trustworthiness of LVLMs for practical applications.

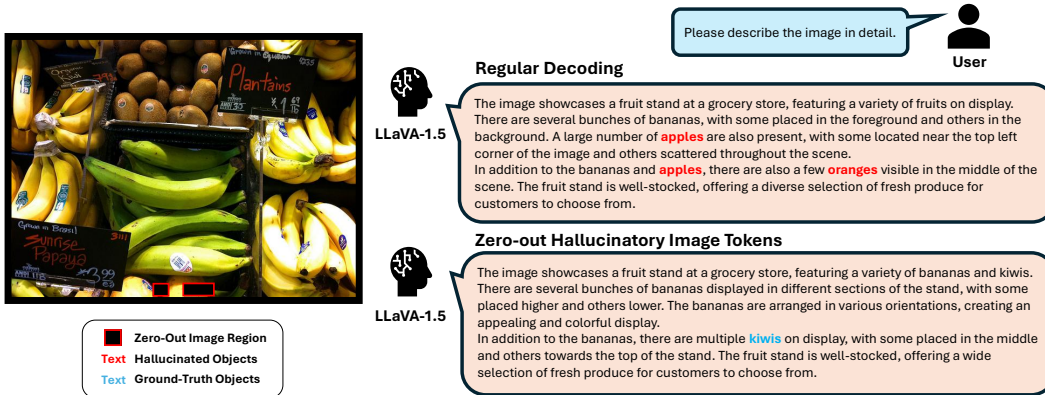


Figure 1: Removing three image tokens results in the elimination of the hallucinated objects, "apples" and "oranges", and reveals the real object "kiwis".

Various studies [Rohrbach et al., 2018, Sun et al., 2023, Guan et al., 2024] have been conducted to investigate the underlying causes of OHs in LVLMs. A significant portion of existing research attributes this issue to the biases from the language part. In [Li et al., 2023, Leng et al., 2024, Zhou et al., 2023], the authors argue that statistical biases in the textual training data are a major contributing factor. These biases include the long-tailed distribution of object occurrence frequencies [Li et al., 2023] and the co-occurrence relationships between different objects [Rohrbach et al., 2018, Zhou et al., 2023]. Some other works [Leng et al., 2024, Lee et al., 2023, Wang et al., 2023b] believe that prior knowledge from the powerful language model overrides input information, resulting in various hallucinations. Consequently, these studies employ contrastive decoding [Li et al., 2022], which achieves decoding correction by comparing token probability distributions before and after modification to image input. Another line of research noticed that the language model pays less attention to the image tokens but more to the most recent text token during the generation process therefore applying generation backtracking [Huang et al., 2024, Wei and Zhang, 2024]. While these pioneering efforts have provided valuable insights into the causes of visual hallucinations, a key question remains: *How does visual input influence the generation of visual hallucinations?* This study aims to explore this critical aspect in depth to better understand hallucination phenomena from the vision perspective.

To address this gap, we investigated how LVLMs process visual inputs and how this contributes to visual OHs. Although using the distribution of attention weights to interpret visual token contributions is a straightforward approach [Neo et al., 2024, Gong et al., 2024, Woo et al., 2024], many layers exhibit noisy attention patterns with no clear correlation between generated object-related tokens and specific image regions. Through a comprehensive analysis of different layers, as shown in Figure 3, we found that LLaVA and similar models predominantly extract object information in their middle-to-late layers. For example, in LLaVA-1.5 (7b), a 32-layer transformer model, we reveal that in the middle layers, such as Layer 15, the generated object tokens assign a large proportion of their attention weights to their visual grounding regions, as shown in Figure 2. This phenomenon effectively links generated object-related tokens to precise regions in the input image and is notably absent in the earlier and final layers. This insight allows us to pinpoint where the model “looks” in the input image while generating text tokens.

Equipped with this analytical tool, we found that real objects tend to focus their attention on their corresponding image anchor regions. In contrast, hallucinatory objects, lacking a true image anchor, concentrate their attention on visually related regions. For example, a nonexistent *baseball glove* could focus its attention on the *baseball* in the image. This finding highlights the critical role of visual bias in generating object hallucinations. When the image anchor of a real object is masked, the model fails to recognize the object. Inspired by this, we apply a *zero-out* operation to the top- K image tokens with the highest attention scores for hallucinated objects, replacing them with zero embeddings. Surprisingly, these hallucinated objects disappear from the new response. We further identified certain image tokens among the top- K zeroed-out tokens—termed **Hallucinatory Image Tokens (HITs)**—that play a key role in generating object hallucinations. As shown in Figure 1,

the hallucinated object could be eliminated by removing even two or three HITs. In contrast, we found that real objects remain largely unaffected by the zero-out operation. This distinction shows a promising way to both detect and mitigate object hallucination.

To evaluate the generalizability of this finding, we curated a dataset of hallucination cases and applied the top- K candidate HITs zero-out operation. The results show that we can successfully reduce most OHs while preserving accurate predictions for real objects. We extended these findings and proposed a novel method, EAZY, which can detect and Eliminate object hAllucination by Zeroing-out hallucinatorY image tokens. EAZY first identifies hallucinated objects in the generated text by removing object-specific top- K candidate HITs, with a detection rate up to 80%. After the hallucination detection stage, the EAZY will rectify the generated response by zeroing out the aggregated HIT candidates from all the detected HOs. Our experiment results show that EAZY surpassed the performance of state-of-the-art (SOTA) training-free methods.

Our contributions can be summarized as below:

- We show that the LVLMs extract object-related information from the visual input in the early middle to late middle layers. This relationship builds strong connections between visual regions and generated object tokens, allowing object localization via attention distribution.
- We discovered an interesting and significant phenomenon: Most HOs generated by LVLMs are directly linked to only a subset of image tokens receiving high attention scores. By zeroing out these *hallucinatory image tokens*, the associated HOs can be eliminated.
- By further validation of the HITs phenomenon, we found that zeroing out top- K candidate HITs not only removes the majority of HOs but has minimal impact on real objects. We propose to use the HITs phenomenon for OH detection, achieving nearly 80% accuracy and precision for both real and hallucinatory objects.
- We propose a method named EAZY for detecting and mitigating OH by zeroing out candidate HITs. Our experimental results demonstrate that the proposed method can adapt to various LVLMs and outperforms state-of-the-art baseline approaches across most evaluation metrics.

2 Connecting Generated Object Token with Its Image Anchor via Attention

We consider LVLMs represented by LLaVA[Liu et al., 2024c], with a model architecture consisting of a vision encoder, a vision-text connecting module, and a transformer-based large language model as the text decoder. An input image I is first divided into N fixed-size patches and then processed by ViT f_V and a linear projector or MLP into a sequence of image tokens. For LLaVA-1.5, a single image will be mapped as 576 image tokens for the LLM decoder.

Given an input sequence $\mathbf{x} = (x_0, x_1, \dots, x_{M+N-1})$, the text decoder $p(x_t|\mathbf{x}_{<t}) = f_T(\mathbf{x}_{<t}|\theta)$ gives the probability distribution of next token over the vocabulary space. Here, M is the text token number; θ are the model parameters; $\mathbf{x}_{<t}$ is the input sequence that contains the tokens prior to the t -th token x_t . The complete generated token sequence \mathbf{x}_{output} is obtained via $F_T(\mathbf{x}|\theta)$. We denote \mathbf{x}_V as input image tokens and \mathbf{x}_T as the input text tokens.

For a token x_i , its representation $h_i^l \in \mathcal{R}^{d_m}$ at the layer l of the text decoder is updated through multi-head self-attention (MHSA) and feed-forward (FF) sublayers with residual connection. Specifically, for the MHSA sublayer with H heads, each head applies self-attention as:

$$\text{Attention}(Q, K, V) = \text{softmax}\left(\frac{QK^T}{\sqrt{d_h}} + M\right)V \quad (1)$$

Here $Q, K, V \in \mathcal{R}^{n \times d_k}$ are the query, key, and value matrices linearly projected from the input; $M \in \mathcal{R}^{n \times n}$ is the casual mask. We utilize the average softmax output of the self-attention $a^l = \text{softmax}\left(\frac{QK^T}{\sqrt{d_n}} + M\right)$ as the attention scores at layer l . We denote the casual self-attention scores from the token x_i to x_j at layer l as a_{ij}^l .

2.1 Evaluating Object Localization Performance among Model Layers.

Understanding how LVLMs process visual input is still in its early stages. Recent studies [Gong et al., 2024, Woo et al., 2024] have preliminarily revealed that models such as LLaVA assign a higher

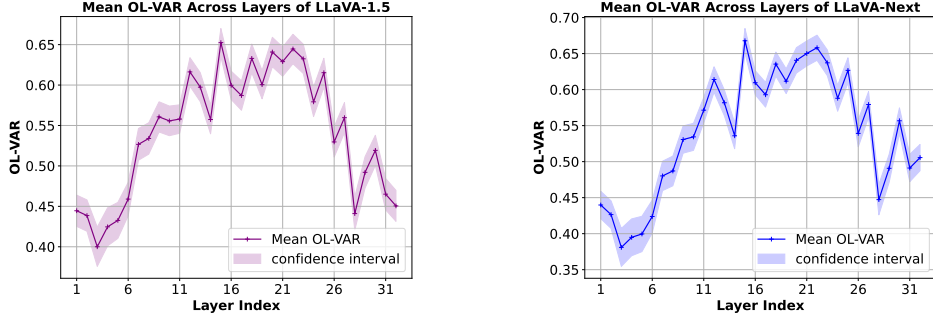


Figure 2: Average OL-VAR over 500 randomly selected MSCOCO images of LLaVA-1.5(left) and LLaVA-Next(right).

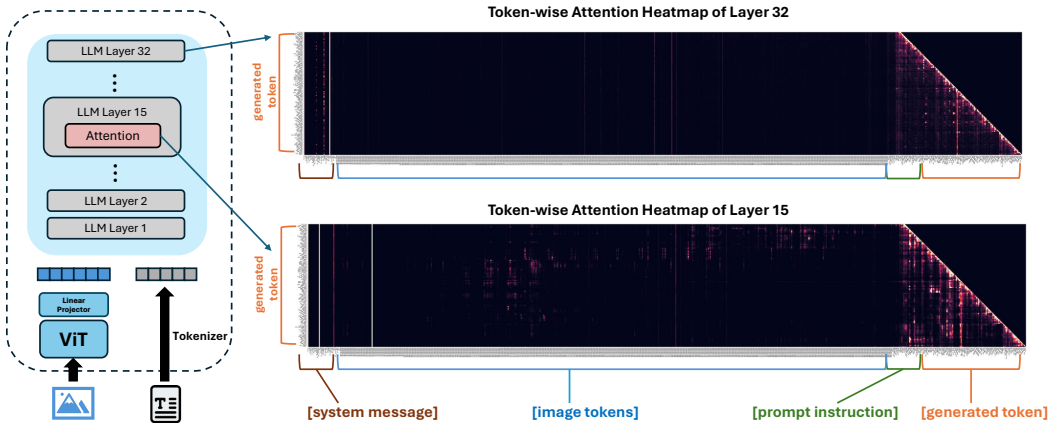


Figure 3: The token-wise attention heatmap of layer 32 and 15 from the LLaVA model. The attention distribution in layer 15 illustrates the connection between the generated object tokens and image tokens, indicating the model extracts object information from the image at the middle layers.

proportion of attention weights over the image tokens in their middle to late layers. However, these analyses fail to identify a clear dependency between the generated object-related tokens and specific image regions within the cluttered, layer-by-layer attention distributions.

To explore where the model establishes connections between the generated object text tokens and their corresponding image regions, i.e., image anchors, we evaluated the performance of object localization using token-to-token attention relationships at each layer. To quantitatively assess the relationship between generated object tokens and their corresponding image regions, we introduced a new metric, the Object Localization Visual Attention Ratio (OL-VAR), to represent the ratio of attention scores over the object bounding box region to all the image tokens by generated object token x_i in layer l :

$$\text{OL-VAR}_i^l = \frac{\sum_{x_k \in \mathbf{x}_{V_O}} a_{ik}^l}{\sum_{x_j \in \mathbf{x}_V} a_{ij}^l}. \quad (2)$$

Here, \mathbf{x}_V represents the set of all the image tokens and \mathbf{x}_{V_O} is the set of image tokens contained in the ground truth bounding box of the target object O . We randomly selected 500 MSCOCO images containing annotated objects and their corresponding bounding boxes and show their average OL-VAR over each layer of LLaVA-1.5 and LLaVA-Next in Figure 2. It can be seen that the model assigns more than 55% of the visual attention weights on the anchors of the object-related image from layer 10 to 25, where layer 15 obtained the highest score OL-VAR. This result offers a new perspective on understanding how LLMs extract object information from visual inputs, revealing that the model primarily extracts and comprehends object information in the early-middle to later-

middle layers. In addition, it provides an effective analytical tool for establishing connections between visual inputs and generated tokens.

We further validated this finding through the visualization of attention heatmaps. In Figure 3, we present two representative token-wise attention heatmaps of LLaVA-1.5 7b with 32 transformer layers. The top panel shows the attention distribution for Layer 32, while the bottom panel depicts the distribution for Layer 15, the layer with the highest OL-VAR on objects. For any given image input, the attention heatmaps of most layers exhibit patterns similar to those of Layer 32. Specifically, the attention scores from generated tokens to the image tend to concentrate on a few specific image tokens, forming an *attention sink* pattern [Xiao et al., 2023]. In contrast, the attention heatmap of Layer 15 exhibits a markedly different distribution. The amount of attention sink pattern is significantly diminished. Instead, multiple distinct attention spots emerge, connecting the generated text tokens with various image tokens. This indicates a more distributed attention mechanism at layer 15, enabling richer interactions between text and visual elements.

3 Object Hallucination from Image Tokens.

This section presents a new perspective on the causes of hallucinations. We found that the presence of hallucinated objects in the generated text is directly correlated with the few image tokens that receive the highest attention scores. We illustrate more details about the distribution of text-to-image token attention in Appendix E.

3.1 Identify Hallucinatory Image Tokens

We begin with a case study where the model is prompted to describe an image of “*a fruit stand with bananas and kiwis*”, as shown in Figure 1. The discovery in Section 2 provides a tool for connecting generated object tokens with their visual grounding. Erasing the image anchor region of a real object prevents the model from recognizing its presence. Inspired by this, we selected the top five image tokens that received the highest attention scores for the hallucinatory objects "apple" and "orange" in the original generation and replaced them with zero embeddings (14 image tokens from multiple HO tokens). Surprisingly, "apple" and "orange" disappeared, while the real object "kiwi" emerged.

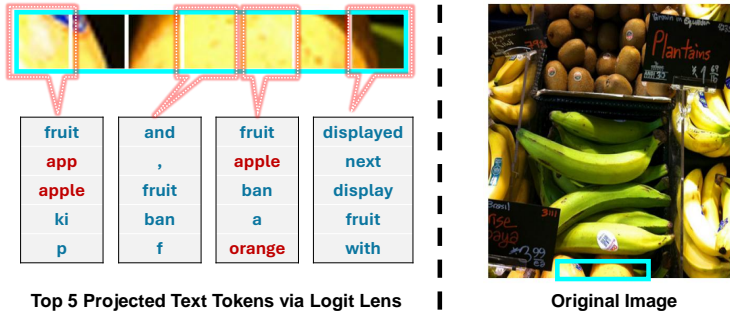


Figure 4: Logit Lens [nostalgebraist, 2020] interpretation of HITs. We display the top-5 projected words of image tokens related to HOs. The HITs are interpreted as the hallucinatory objects, "apple" and "orange".

Our further analysis aims to identify the smallest set of image tokens capable of eliminating hallucinations. Ultimately, we identified three key image tokens among the top-attended tokens, located in the lower part of the 'papaya' region. Remarkably, zeroing out just these three tokens achieved the same effect as removing all 14 image tokens with high attention scores. To further investigate how the LLM interprets these image tokens, we applied the Logit Lens [nostalgebraist, 2020] technique, which maps the hidden states of image tokens to the LLM’s vocabulary space. In Figure 4, we show the top-5 projected vocabulary words associated with several image tokens in the papaya region. Surprisingly, the three key image tokens are interpreted as "apple" and "orange" by Logit Lens. This aligned with our initial observation that certain image tokens are directly associated with hallucinatory objects because of inherent visual biases. We define this type of image tokens as the *Hallucinatory*

Image Tokens (HITs)¹. In the next section, we demonstrate that zeroing out the top- K candidate HITs (top- K most attended image tokens by HOs) can universally reduce object hallucination across different images and contexts.

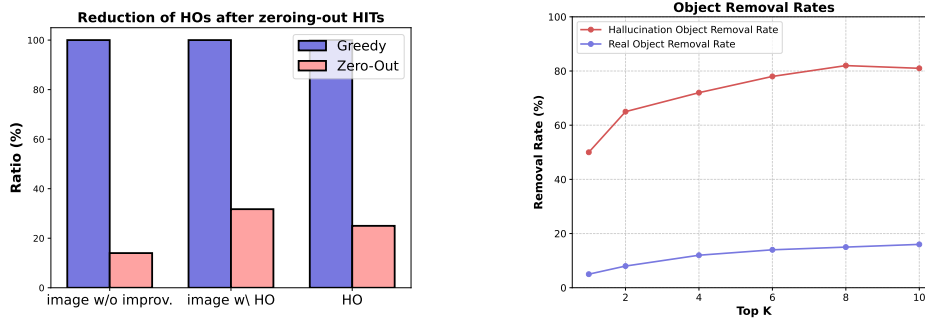


Figure 5: **Left:** Reduction ratio of OHs in Hall-COCO after zeroing-out HITs. We show the ratio changes of image w/o improv.(ratio of images with the same HOs after zeroing out), image w OH (images with OH in the response), and HO (Ratio of HOs in all text responses). **Right:** The fraction change of real and hallucinatory objects removed by zeroing out the top- K candidate HITs.

3.2 Quantifying the Impact of Zeroing Out HITs

To further validate that the HITs phenomenon is broadly applicable, we curated a dataset named *Hall-COCO*, containing 200 images from MSCOCO dataset [Rohrbach et al., 2018] that consistently induce object hallucinations identified by human annotation. We provide more details in Appendix A.

We evaluate how zero-out the candidate HITs (top attended image tokens by HO tokens) will impact the number of object hallucinations in the model’s responses. As presented in Figure 5 Left, we can see that after zero-outing the top 5 candidate HITs with the same greedy decoding, 86% of images got improved description with less hallucination. The proportion of images with hallucination decreased from 100% to 31.73%. 74.17% of the object hallucination directly disappeared from the updated generation. This verified that most hallucinatory image tokens are part of the image tokens that received the most attention weights from the OH tokens. Removing these top- K candidate hallucinatory image tokens leading to the removal of OH can be widely applied to different images.

3.3 Real Objects are Robust to Zero-Out

We demonstrate that zeroing out hallucinatory image tokens significantly reduces the generation of hallucinated object tokens. This raises an interesting question: What is the effect of zeroing out high-attention patches for real objects? To explore this, we evaluate the impact of zeroing out the top- K HITs on both hallucinated and real objects. Specifically, we measure the fraction of objects removed by counting how many objects remain in the model response after removing the top- K image tokens with the highest attention scores from the corresponding text object token, relative to the total number of objects. The results, shown in Figure 5 (Right), reveal that object hallucinations are highly sensitive to zeroed HITs. For example, when $K = 8$, approximately 80% of hallucinated objects were successfully eliminated, while only a small fraction (10%) of real objects were affected. Notably, the few real objects that were removed tended to be small or positioned at the periphery of the image. We provide a failure case study in Appendix F.

4 Detecting and Mitigating Object Hallucination by HIT Zero-outs

In this section, we introduce our proposed methods, EAZY (Eliminate object hAllucination by Zero-out hallucinatorY image tokens), an automatic approach to detect and mitigate object hallucinations in LVLMS.

¹Logit Lens alone cannot capture all HITs. Interpretability-based methods for detecting such tokens could offer improved alignment, and we plan to consider alternate tools to refine this approach in the future.

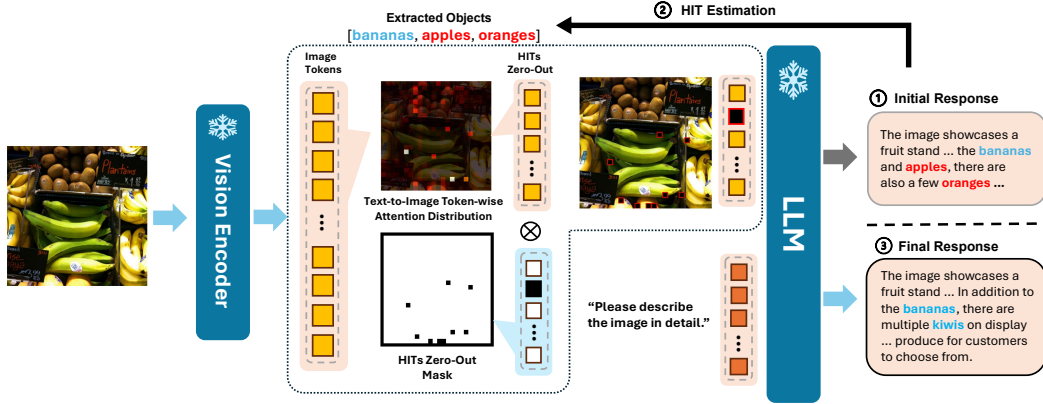


Figure 6: Overview of the proposed EAZY method. The process starts with an image input encoded into image tokens. The LLM generates an initial response with hallucinated objects (**apples**, **oranges**). EAZY estimates HITs via text-to-image token-wise attention distribution. With HITs zeroed out, the final response has the hallucinations disappeared, revealing correct objects (**kiwis**).

4.1 Object Hallucination Detection

Our results in Section 2 and 3 indicate that removing the top- K candidate HITs from consideration effectively eliminates HO in the revised model output, while largely preserving the integrity of real objects. Leveraging this differentiation between genuine and HO tokens, we suggest identifying OH by discarding the top- K candidate HITs.

Given an image input I and its corresponding input token sequence \mathbf{x}_I , the text decoder produces G generated tokens $\mathbf{x}_{output} = \{x_{M+N}, \dots, x_{M+N+G-1}\}$. We then utilize pre-built NLP techniques such as POS tagging and dependency parsing [Bird, 2006] to extract object tokens in the generated response \mathbf{x}_{output} , resulting in a subset \mathbf{x}_{obj} . For any $x_i \in \mathbf{x}_{obj}$, let a_{ij} represent the attention score of x_i on an image token x_j . The zero-out token set \mathbf{z}_i is defined as

$$\mathbf{z}_i = \{x_j \in \mathbf{x}_I \mid j \in \arg \text{top}_K(\{a_{ij} \mid x_j \in \mathbf{x}_I\})\}, \quad (3)$$

where $\arg \text{top}_K$ selects the indices of the K largest attention scores $\{a_{ij} \mid x_j \in \mathbf{x}_I\}$. We modify the image input by applying zero-out based on \mathbf{z}_i ,

$$\mathbf{x}_{input}^{\mathbf{z}_i} = \{x_j \leftarrow \mathbf{0}_{d_m} \mid x_j \in \mathbf{z}_i\}. \quad (4)$$

Here, $\mathbf{x}_{input}^{\mathbf{z}_i}$ indicates the input sequence with the tokens in \mathbf{z}_i replaced by zeroing embedding $\mathbf{0}_{d_m} \in \mathcal{R}^{d_m}$. We check the updated generation result \mathbf{x}_{output}^i by text decoder $\mathbf{x}_{output}^i = F_T(\mathbf{x}_{input}^{\mathbf{z}_i} \mid \theta)$. If $x_i \notin \mathbf{x}_{output}^i$, EAZY classifies x_i as an object hallucination, and a real object otherwise.

4.2 Mitigating Object Hallucination

As shown in Figure 6, the mitigation application of EAZY starts from an initial inference without intervention. Following a similar process as the detection application, the object tokens x_{obj} are extracted from the initial response. We then group the top- K candidate HITs $\mathcal{Z}_I^{estimate}$ for all objects $x_i \in \mathbf{x}_{obj}$ and apply zero-out to the image tokens accordingly. The model then performs inference for HITs estimation after zeroing out the corresponding image tokens. EAZY identifies objects that disappear in the new response as hallucinatory object tokens \mathbf{x}_{obj}^{HO} .

We collect all the top- K candidate HIT sets of the HO tokens detected from the previous HIT estimate stage. We take the union set of all the candidate HITs sets to obtain the final zero-out token list \mathcal{Z}_I^{final} , which is defined as

$$\mathcal{Z}_I^{final} = \bigcup_{x_i \in \mathbf{x}_{obj}} \mathbf{z}_i \quad \text{where } x_i \in \mathbf{x}_{obj}^{HO}. \quad (5)$$

Algorithm 1 EAZY

Require: Image input I , text decoder F_T , attention scores a_{ij} , top- K threshold K **Ensure:** Mitigated response \mathbf{x}_{output} 1: Compute initial response: $\mathbf{x}_{output} \leftarrow F_T(\mathbf{x}_I | \theta)$ 2: Extract object tokens: $\mathbf{x}_{obj} \leftarrow \mathbf{x}_{output}$ 3: Identify top- K attended tokens for all objects:

$$\mathcal{Z}_I^{estimate} = \bigcup_{x_i \in \mathbf{x}_{obj}} \arg \text{top}_K(\{a_{ij} | x_j \in \mathbf{x}_{obj}\})$$

4: Zero-out all hallucinated tokens: $\mathbf{x}_{input}^{\mathcal{Z}_I^{estimate}} \leftarrow \mathbf{x}_I$ with $\mathcal{Z}_I^{estimate}$ replaced by $\mathbf{0}_{d_m}$ 5: Generate updated response: $\mathbf{x}_{output}^{HIT} = F_T(\mathbf{x}_{input}^{\mathcal{Z}_I} | \theta)$ 6: Identify hallucinated objects: $\mathbf{x}_{obj}^{HO} = \{x_i \in \mathbf{x}_{obj} | x_i \notin \mathbf{x}_{output}^{HIT}\}$

7: Final zero-out of hallucinated tokens:

$$\mathcal{Z}_I^{final} = \bigcup_{x_i \in \mathbf{x}_{halluc}} \arg \text{top}_K(\{a_{ij} | x_j \in \mathbf{x}_I\})$$

8: Generate final response: $\mathbf{x}_{output}^{EAZY} = F_T(\mathbf{x}_{input}^{\mathcal{Z}_I} | \theta)$ **return** \mathbf{x}_{output}

The model then utilizes the final zero-out token list \mathcal{Z}_I^{final} to replace all the candidate hallucinatory image tokens by zero embedding for the final generation:

$$\mathbf{x}_{output}^{EAZY} = F_T(\mathbf{x}_{input}^{\mathcal{Z}_I^{final}} | \theta). \quad (6)$$

5 Experiment

In this section, we conduct experiments on multiple datasets and metrics to validate the superior performance of EAZY in detecting and mitigating hallucinated objects (HOs).

METHOD	LLAVA-1.5		SHIKRA		LLAVA-NEXT	
	CHAIR _S ↓	CHAIR _I ↓	CHAIR _S ↓	CHAIR _I ↓	CHAIR _S ↓	CHAIR _I ↓
GREEDY	49.6	14.4	55.8	15.4	32.8	9.1
BEAM SEARCH	46.3	12.9	50.4	13.3	33.0	9.2
DOLA	47.1	13.8	55.4	15.7	31.3	9.0
VCD	49.2	14.8	56.4	15.5	32.8	8.9
OPERA	45.4	12.7	46.2	13.1	34.0	8.7
SID	44.2	12.2	44.8	12.8	32.8	8.3
EAZY	38.8	11.4	26.6	8.9	26.8	8.3

Table 1: **Evaluation Results with CHAIR.** The lower, the better.

METHOD	LLAVA-1.5		SHIKRA		LLAVA-NEXT	
	Acc ↑	F1 ↑	Acc ↑	F1 ↑	Acc ↑	F1 ↑
GREEDY	81.38	82.20	80.87	81.05	83.78	82.24
BEAM SEARCH	84.66	84.60	80.48	81.81	83.77	81.69
DOLA	84.06	84.62	80.71	81.19	84.53	84.77
VCD	84.66	84.52	79.87	81.06	83.37	83.95
OPERA	84.88	85.21	79.99	81.48	84.37	84.21
SID	84.82	85.50	80.02	81.23	84.61	85.32
EAZY	84.97	85.78	80.96	82.38	84.91	85.40

Table 2: **Evaluation Result on POPE.** We take the average accuracy and F1 score of random, popular, and adversarial modes.

5.1 Experiment Setting

5.1.1 OH Mitigation Setting

Model. We choose the LLaVA-1.5 [Liu et al., 2024a], Shikra [Chen et al., 2023] at 7B scale and LLaVA-Next [Liu et al., 2024b] at 8B scale for evaluation of OH mitigation. We set the maximum number of generated tokens as 512 in our setting. Please refer to Appendix B.1 for more model details.

Baseline. We compare our method EAZY with six *training-free* methods including three LLM decoding strategies, greedy and beam search and Dola [Chuang et al., 2024], as well as three state-of-the-art hallucination mitigation methods for LVLm, VCD [Leng et al., 2024], OPERA [Huang et al., 2024] and SID [Huo et al., 2025]. We adopt greedy decoding for Dola, SID and EAZY. We set the beam number as 5 and apply sampling for VCD and OPERA. We provide more implementation details in Appendix B.2.

Metric. The Caption Hallucination Assessment with Image Relevance (CHAIR) [Rohrbach et al., 2018] is an evaluation tool designed to assess object hallucination issues in the image captioning task. CHAIR quantifies the degree of object hallucination from sentence-level, $CHAIR_S$, and image-level, $CHAIR_I$, which are calculated by the ratio of hallucinated objects and the ground-truth label objects. Specifically, CHAIR is calculated as:

$$CHAIR_S = \frac{|\{\text{hallucinated objects}\}|}{|\{\text{all mentioned objects}\}|}, \quad (7)$$

$$CHAIR_I = \frac{|\{\text{captions w/ hallucinated objects}\}|}{|\{\text{all captions}\}|} \quad (8)$$

Polling-based Object Probing Evaluation (POPE) [Li et al., 2023] is a metric designed to evaluate object hallucination in LVLms. During evaluation, POPE prompts LVLm with straightforward Yes-or-No questions about the presence of specific objects in an image (e.g., "Is there an apple in the image?") POPE offers three evaluation settings: *Random*, *Popular*, and *Adversarial*. In Random Sampling, objects that do not exist in the image are selected randomly. In Popular Sampling, the top- k most frequent objects in the entire image dataset that are absent from the current image are selected, where $k = \lfloor n/2 \rfloor$. Lastly, Adversarial Sampling ranks objects by their co-occurrence frequency with ground-truth objects and selects the top- k frequent ones that are not in the image. In our experiment, we show the average accuracy and F1 score result over three different sampling modes on the MSCOCO dataset [Lin et al., 2014].

5.1.2 OH Detection Setting

Baselines. We chose two state-of-the-art *training-free* OH detection methods as baselines to compare our method on Hall-COCO. Uncertainty (UT) [Zhou et al., 2023] found that HOs often exhibit higher uncertainty scores during generation. Internal Confidence (IC) [Jiang et al., 2024] found the maximum logit lens probability can be utilized for OH detection.

Model and Benchmark. We evaluate different OH detection methods on the LLaVA-1.5 7B model with greedy decoding. The maximum length of the generation is 512 tokens. We use Hall-COCO as the benchmark for the open-end image description task. Each image has human-annotated real and hallucinatory objects.

Metric. We follow [Jiang et al., 2024] to treat the OH detection as a binary classification task, where real objects are the positive class and HOs as the negative. We use accuracy (Acc), precision (PR), recall, and F1 score as the evaluation metrics.

5.2 Evaluation

5.2.1 Evaluation Result on OH Mitigation

We adopt CHAIR [Rohrbach et al., 2018] and POPE [Li et al., 2023] as quantitative metrics to compare the hallucination mitigation performance between the proposed EAZY and baseline methods. For the CHAIR result in Table 1, we follow [Huang et al., 2024, Huo et al., 2025, Gong et al., 2024, Favero et al., 2024] to evaluate different LVLms with 500 randomly selected images from

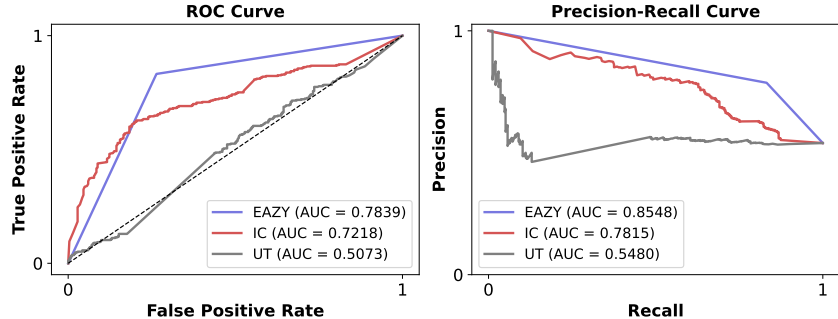


Figure 7: **Object Hallucination Detection Curves on Hall-COCO.** We present the Precision-Recall and ROC curves of the proposed OH detection method and baselines.

METHOD	ACC	PR(RO)	PR(OH)	RECALL	F1
UT	50.57	53.60	42.77	70.62	60.95
IC	62.56	61.93	64.16	81.6	70.42
ZERO-OUT	78.77	78.41	79.25	83.38	80.82

Table 3: **OH Detection Results on Hall-COCO.** PR(RO) represents the precision of real objects (positive instances), while PR(OH) represents the precision of object hallucination (negative instances). **UT** [Zhou et al., 2023] is the uncertainty detection method. **IC** [Jiang et al., 2024] is the internal confidence method.

MSCOCO [Lin et al., 2014] with the fixed prompt: “Please describe this image in detail.”. The proposed method EAZY surpasses the baselines by a large margin for three different LVLMs, validating the effectiveness of EAZY in open-end generation tasks. We show the average evaluation results on POPE in Table 2, which comprises three datasets. EAZY attains the best average performance in random, popular, and adversarial sampling settings, outperforming all other methods. It can be observed that, under the POPE metric, the advantage of EAZY is not as pronounced as in the CHAIR results. We attribute this to the binary Yes-or-No question format of POPE, which may lead to generated content that does not include object tokens. Furthermore, the prompt “Is there an object in the image?” already contains the object name, potentially impacting models’ attention distribution.

5.2.2 Evaluation Result on OH Detection

We present the quantitative results of OH detection on LLaVA-1.5 in Table 3 and Figure 7. We find that EAZY improves the accuracy 16.21%, 16.48% in the precision of real objects, and 15.09% in the precision of HO, compared to the best baseline. In addition, EAZY improves the ROC AUC by 8.60% and the PR AUC by 9.37% over the baseline. This indicates the superior performance of EAZY on OH detection with a good balance of precision on both real and hallucinatory objects. We provide additional results for LLaVA-Next and Shikra models in Appendix B.4.

5.3 Ablation Study

Impact of K value selection. The choice of the value K is critical to the mitigation performance of EAZY. In Figure 8, we show the impact of different values K for the LLaVA-1.5 and Shikra models on the CHAIR metric. We use the Greedy decoding performance as the reference line. It can be seen that LLaVA-1.5 achieves the best performance when $K = 5$ and Shikra is on $K = 3$.

Impact of Zero-Out Position in the Pipeline. In EAZY, we apply the zero-out of image tokens in the LLM input space, i.e., replace the target image tokens with zero embeddings. To transform the original image into image tokens, the LVLMs first utilize the ViT to process the image from image patches into patch embeddings, then use the linear projector or MLP to map the patch embeddings into image tokens. We apply the zero-out operation on three different positions in the image processing pipeline, including the input token space, the output space of ViT, and the original image patches. As shown in Table 4, applying the zero-out operation at different positions on the same set of image

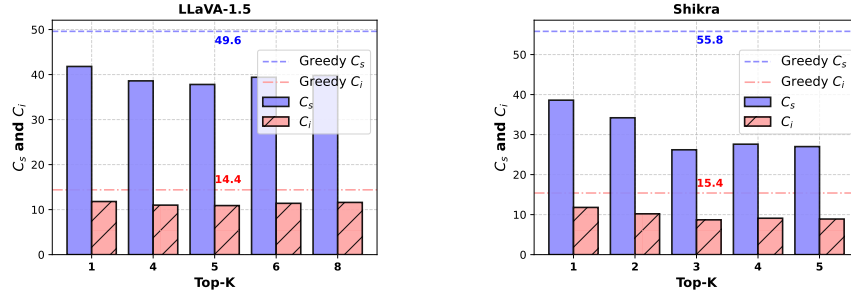


Figure 8: CHAIR evaluation results as a function of K on LLaVA-1.5 (left) and Shikra (right).

POSITION	CHAIR _S ↓	CHAIR _I ↓
INPUT TOKEN	38.8	11.4
VIT OUTPUT	40.4	11.8
IMAGE PATCHES	39.0	11.4

Table 4: Evaluation Result of Different Zero-Out Positions on CHAIR.

tokens (or patch embeddings) effectively mitigates object hallucination in the model response. This suggests that the visual biases introduced by hallucinatory image tokens originate directly from the image itself and are not strongly associated with modules such as ViT or Linear Projector.

METHODS	IMAGE W/O OH	REMOVED OH
ZERO-OUT	68.27%	74.17%
AVERAGE	55.17%	66.67%
RANDOM	58.56%	63.33%
NEIGHBOR	55.17%	61.25%

Table 5: Evaluation Result of Top-K Image Token Processing Strategies on Hall-COCO.

Impact of Image Token Processing Strategies. We explored how the different processing methods for the top-K image tokens impact the removal of object hallucination (OH). In Table 5, we show the performance of four different processing strategies on the collected *Hall-COCO* dataset when $K = 5$. The zero-out method, which is used in EAZY, replaces the embeddings of the top-K candidate HITs with zero embeddings. The average method replaces the top-K most attended image token embeddings with the average embedding of all the image tokens. The random method replaces the token embeddings of top-K candidate HITs with a randomly selected image token embedding. The neighbor method replaces the top-K candidate HITs embeddings with one of their neighbor image tokens adjunct to the target image token. Overall, our zero-out performs better in the percentage of images without object hallucinations and removed object hallucinations compared to alternative strategies.

Statistic on Image Token Zeroing-out

We measured the average number of image tokens zeroed out when applying EAZY across different LVLMS, as well as the ratio of this number to the total image tokens. As shown in Table 6, LLaVA-1.5 zeroes out an average of 8.98 image tokens out of 576, resulting in a ratio of 1.56%. Shikra removes 5.23 image tokens on average from a total of 256, yielding a slightly higher ratio of 2.04%. LLaVA-Next, which processes significantly more image tokens (2880 in total), removes an average of 40.95 tokens, with a ratio of 1.42%. These results demonstrate that EAZY requires modifying only a small fraction of image tokens to effectively mitigate hallucinations, highlighting its efficiency and minimal impact on the overall visual representation.

MODEL	LLAVA-1.5	SHIKRA	LLAVA-NEXT
# AVERAGE ZEROED-OUT	8.98	5.23	40.95
# TOTAL IMAGE TOKEN	576	256	2880
RATIO	1.56%	2.04%	1.42%

Table 6: The statistic result of the average zeroed-out image token numbers by EAZY, the total number of image tokens and the ratio between them for each model.

6 Related Work

Large Vision-Language Models. Recent progress in integrating advanced LLMs [Chiang et al., 2023] with foundation models such as CLIP [Radford et al., 2021] has significantly enhanced the capabilities of these Large Vision Language Models (LVLMs), allowing them to complete various vision tasks following prompt instruction. These powerful LVLMs usually contain a vision model to encode visual input, a cross-modal connection module to map the image features into text input space, and an LLM decoder for multi-modal input. LLaVA-1.5 [Liu et al., 2024c] is one of the most representative LVLM that utilizes a linear layer as the connection module. This achieves a one-to-one mapping from the image patch to the 576 image tokens. Shikra [Chen et al., 2023] adapted a similar architecture while mapping the image input to 256 image tokens. LLaVA-NEXT [Liu et al., 2024a] is improved based on the previous LLaVA model, using MLP as the connector and utilizing the AnyRes technique to generate 2880 image features with expanded instruction tuning datasets. Despite continuous improvement of the LVLMs, all of these models suffer from severe object hallucination problems. In this work, we focus on the analysis, detection, and mitigation of object hallucinations in these models.

Cause of Object Hallucination. Hallucination [Bai et al., 2024] affects the trustworthiness and reliability of LVLM for broad application. Specifically, object hallucination [Rohrbach et al., 2018], which refers to describing HOs in the input images, is more harmful than other types of inaccurate description. Recent studies have proposed explaining the causes of hallucination from training data biases [Zhou et al., 2023, Wang et al., 2023a, Yu et al., 2024] and language biases [Leng et al., 2024, Favero et al., 2024, Huang et al., 2024, Lee et al., 2023]. In [Liu et al., 2025, Favero et al., 2024], the authors found that LVLMs exhibit a preference for text tokens, causing the model to pay more attention on neighboring text tokens when generating new tokens.

Mitigation of Object Hallucination. Due to the complex structure and the large number of parameters in LVLMs, addressing hallucinations through retraining or fine-tuning is often prohibitively expensive and computationally intensive. As a result, many studies focus on mitigation during inference. A series of decoding strategy-based works [Leng et al., 2024, Woo et al., 2024, Wei and Zhang, 2024, Favero et al., 2024] leverage contrastive decoding technique [Li et al., 2022] to compare the model’s original logit probability distribution with the logit output generated from processed images, thereby suppressing prior knowledge biases and statistical biases introduced by the training data. Meanwhile, methods such as OPERA [Huang et al., 2024] and DAMRO [Gong et al., 2024] have observed that sequence supervision-induced anchor tokens significantly increase the likelihood of hallucinations in subsequent tokens. Compared to these works, we discovered that visual biases are the cause of most object hallucinations and developed a simple yet effective method by zeroing out the hallucinatory image tokens.

7 Conclusion

In this paper, we identify a new cause of object hallucination from the perspective of visual bias—Hallucinatory Image Tokens. A small number of image tokens with high attention scores are directly correlated with the presence of hallucinated objects in the generated text. Replacing these HITs with zero embeddings effectively removes hallucinated objects while minimally affecting real objects. Based on this finding, we propose EAZY, a training-free method for automatically detecting and mitigating object hallucinations. Through extensive experiments, we demonstrate the superior performance of EAZY in both hallucination detection and mitigation. We provide more discussion and visualization results in Appendix G and H.

References

- Z. Bai, P. Wang, T. Xiao, T. He, Z. Han, Z. Zhang, and M. Z. Shou. Hallucination of multimodal large language models: A survey. *arXiv preprint arXiv:2404.18930*, 2024.
- S. Bird. Nltk: the natural language toolkit. In *Proceedings of the COLING/ACL 2006 Interactive Presentation Sessions*, pages 69–72, 2006.
- K. Chen, Z. Zhang, W. Zeng, R. Zhang, F. Zhu, and R. Zhao. Shikra: Unleashing multimodal llm’s referential dialogue magic. *arXiv preprint arXiv:2306.15195*, 2023.
- W.-L. Chiang, Z. Li, Z. Lin, Y. Sheng, Z. Wu, H. Zhang, L. Zheng, S. Zhuang, Y. Zhuang, J. E. Gonzalez, et al. Vicuna: An open-source chatbot impressing gpt-4 with 90%* chatgpt quality. See <https://vicuna.lmsys.org> (accessed 14 April 2023), 2(3):6, 2023.
- Y.-S. Chuang, Y. Xie, H. Luo, Y. Kim, J. R. Glass, and P. He. Dola: Decoding by contrasting layers improves factuality in large language models. In *The Twelfth International Conference on Learning Representations*, 2024. URL <https://openreview.net/forum?id=Th6NyL07na>.
- A. Favero, L. Zancato, M. Trager, S. Choudhary, P. Perera, A. Achille, A. Swaminathan, and S. Soatto. Multimodal hallucination control by visual information grounding. In *Proceedings of the IEEE/CVF Conference on Computer Vision and Pattern Recognition*, pages 14303–14312, 2024.
- X. Gong, T. Ming, X. Wang, and Z. Wei. Damro: Dive into the attention mechanism of lvlm to reduce object hallucination. *arXiv preprint arXiv:2410.04514*, 2024.
- T. Guan, F. Liu, X. Wu, R. Xian, Z. Li, X. Liu, X. Wang, L. Chen, F. Huang, Y. Yacoob, et al. Hallusionbench: an advanced diagnostic suite for entangled language hallucination and visual illusion in large vision-language models. In *Proceedings of the IEEE/CVF Conference on Computer Vision and Pattern Recognition*, pages 14375–14385, 2024.
- Q. Huang, X. Dong, P. Zhang, B. Wang, C. He, J. Wang, D. Lin, W. Zhang, and N. Yu. Opera: Alleviating hallucination in multi-modal large language models via over-trust penalty and retrospection-allocation. In *Proceedings of the IEEE/CVF Conference on Computer Vision and Pattern Recognition*, pages 13418–13427, 2024.
- F. Huo, W. Xu, Z. Zhang, H. Wang, Z. Chen, and P. Zhao. Self-introspective decoding: Alleviating hallucinations for large vision-language models. In *The Thirteenth International Conference on Learning Representations*, 2025. URL <https://openreview.net/forum?id=rsZwwjYHuD>.
- N. Jiang, A. Kachinthaya, S. Petryk, and Y. Gandselman. Interpreting and editing vision-language representations to mitigate hallucinations. *arXiv preprint arXiv:2410.02762*, 2024.
- S. Lee, S. H. Park, Y. Jo, and M. Seo. Volcano: mitigating multimodal hallucination through self-feedback guided revision. *arXiv preprint arXiv:2311.07362*, 2023.
- S. Leng, H. Zhang, G. Chen, X. Li, S. Lu, C. Miao, and L. Bing. Mitigating object hallucinations in large vision-language models through visual contrastive decoding. In *Proceedings of the IEEE/CVF Conference on Computer Vision and Pattern Recognition*, pages 13872–13882, 2024.
- X. L. Li, A. Holtzman, D. Fried, P. Liang, J. Eisner, T. Hashimoto, L. Zettlemoyer, and M. Lewis. Contrastive decoding: Open-ended text generation as optimization. *arXiv preprint arXiv:2210.15097*, 2022.
- Y. Li, Y. Du, K. Zhou, J. Wang, W. X. Zhao, and J.-R. Wen. Evaluating object hallucination in large vision-language models. *arXiv preprint arXiv:2305.10355*, 2023.
- T.-Y. Lin, M. Maire, S. Belongie, J. Hays, P. Perona, D. Ramanan, P. Dollár, and C. L. Zitnick. Microsoft coco: Common objects in context. In *Computer Vision—ECCV 2014: 13th European Conference, Zurich, Switzerland, September 6–12, 2014, Proceedings, Part V 13*, pages 740–755. Springer, 2014.
- H. Liu, C. Li, Y. Li, and Y. J. Lee. Improved baselines with visual instruction tuning. In *Proceedings of the IEEE/CVF Conference on Computer Vision and Pattern Recognition*, pages 26296–26306, 2024a.
- H. Liu, C. Li, Y. Li, B. Li, Y. Zhang, S. Shen, and Y. J. Lee. Llava-next: Improved reasoning, ocr, and world knowledge, January 2024b. URL <https://llava-vl.github.io/blog/2024-01-30-llava-next/>.
- H. Liu, C. Li, Q. Wu, and Y. J. Lee. Visual instruction tuning. *Advances in neural information processing systems*, 36, 2024c.

- H. Liu, W. Xue, Y. Chen, D. Chen, X. Zhao, K. Wang, L. Hou, R. Li, and W. Peng. A survey on hallucination in large vision-language models. *arXiv preprint arXiv:2402.00253*, 2024d.
- S. Liu, K. Zheng, and W. Chen. Paying more attention to image: A training-free method for alleviating hallucination in vlms. In *European Conference on Computer Vision*, pages 125–140. Springer, 2025.
- C. Neo, L. Ong, P. Torr, M. Geva, D. Krueger, and F. Barez. Towards interpreting visual information processing in vision-language models. *arXiv preprint arXiv:2410.07149*, 2024.
- nostalgebraist. Interpreting gpt: The logit lens, August 2020. URL <https://www.lesswrong.com/posts/AcKRB8wDpdaN6v6ru/interpreting-gpt-the-logit-lens>. Accessed: 2024-12-21.
- OpenAI and A. et al. Gpt-4 technical report, 2024. URL <https://arxiv.org/abs/2303.08774>.
- A. Radford, J. W. Kim, C. Hallacy, A. Ramesh, G. Goh, S. Agarwal, G. Sastry, A. Askell, P. Mishkin, J. Clark, et al. Learning transferable visual models from natural language supervision. In *International conference on machine learning*, pages 8748–8763. PMLR, 2021.
- A. Rohrbach, L. A. Hendricks, K. Burns, T. Darrell, and K. Saenko. Object hallucination in image captioning. *arXiv preprint arXiv:1809.02156*, 2018.
- Z. Sun, S. Shen, S. Cao, H. Liu, C. Li, Y. Shen, C. Gan, L.-Y. Gui, Y.-X. Wang, Y. Yang, et al. Aligning large multimodal models with factually augmented rlhf. *arXiv preprint arXiv:2309.14525*, 2023.
- J. Wang, Y. Wang, G. Xu, J. Zhang, Y. Gu, H. Jia, M. Yan, J. Zhang, and J. Sang. An llm-free multi-dimensional benchmark for mllms hallucination evaluation. *arXiv preprint arXiv:2311.07397*, 2023a.
- J. Wang, Y. Zhou, G. Xu, P. Shi, C. Zhao, H. Xu, Q. Ye, M. Yan, J. Zhang, J. Zhu, et al. Evaluation and analysis of hallucination in large vision-language models. *arXiv preprint arXiv:2308.15126*, 2023b.
- J. Wei and X. Zhang. Dopra: Decoding over-accumulation penalization and re-allocation in specific weighting layer. In *Proceedings of the 32nd ACM International Conference on Multimedia*, pages 7065–7074, 2024.
- S. Woo, D. Kim, J. Jang, Y. Choi, and C. Kim. Don’t miss the forest for the trees: Attentional vision calibration for large vision language models. *arXiv preprint arXiv:2405.17820*, 2024.
- G. Xiao, Y. Tian, B. Chen, S. Han, and M. Lewis. Efficient streaming language models with attention sinks. *arXiv preprint arXiv:2309.17453*, 2023.
- Q. Yu, J. Li, L. Wei, L. Pang, W. Ye, B. Qin, S. Tang, Q. Tian, and Y. Zhuang. Hallucidoctor: Mitigating hallucinatory toxicity in visual instruction data. In *Proceedings of the IEEE/CVF Conference on Computer Vision and Pattern Recognition*, pages 12944–12953, 2024.
- Y. Zhou, C. Cui, J. Yoon, L. Zhang, Z. Deng, C. Finn, M. Bansal, and H. Yao. Analyzing and mitigating object hallucination in large vision-language models. *arXiv preprint arXiv:2310.00754*, 2023.

A Hall-COCO: Benchmarking for Object Hallucination Mitigation Evaluation

To validate that the phenomenon of HITs can be broadly applied to other images, we constructed a dataset, named *Hall-COCO*, from MSCOCO [Lin et al., 2014] where each image reliably induces object hallucination. The dataset creation involved several steps. First, we used GPT-4o [OpenAI and et al., 2024] to detect hallucinations in the output of LLaVA. Next, human annotators identified specific object hallucinations in the model’s responses. For each hallucinated object, we then identified the top 5 image tokens with the highest attention scores. In cases where multiple hallucinated objects were present in the output, we applied a union operation to compile the set of relevant tokens. Through this process, we curated a dataset containing 200 images that consistently induce object hallucinations.

IMAGE	REAL OBJECTS	OH
200	333	284

Table 7: The number of images, real objects and object hallucinations (OH) in Hall-COCO.

B Extended Experiment

B.1 Model Details.

LLaVA-1.5. The LLaVA-1.5 Model [Liu et al., 2024c] leverages the linear projector layer to align the vision and text modalities, with 576 image tokens. It adopted the pre-trained vision transformer from CLIP [Radford et al., 2021] and the pre-trained language model as Vicuna [Chiang et al., 2023].

Shikra. The Shikra Model [Chen et al., 2023] introduces referential dialogue capabilities in multi-modal large language models (MLLMs) by handling spatial coordinate inputs and outputs in natural language. It utilizes a vision encoder, an alignment layer, and a Vicuna-based language model without requiring extra vocabularies, position encoders, pre-/post-detection modules, or external plug-ins. The model enables interaction with images through natural pointing and location-aware responses, supporting tasks such as Referring Expression Comprehension (REC), PointQA, Image Captioning, and Visual Question Answering (VQA) with promising performance.

LLaVA-Next. The LLaVA-Next Model [Liu et al., 2024b] enhances multimodal capabilities by increasing the input image resolution up to 672×672 pixels, supporting three aspect ratios. It utilizes an improved visual instruction tuning data mixture to bolster visual reasoning and OCR capabilities. The model employs a pre-trained vision transformer from CLIP and integrates with advanced language models like Vicuna and Mistral.

B.2 Implementation Detail

For LLaVA-1.5, we use the attention score from layer 15 (index starting from 1) to choose the top-5 most attended image tokens as the candidate HITs. For Shikre, we use the attention score from layer 18 (index starting from 1) to choose the top-3 most attended image tokens as the candidate HITs. For LLaVA-Next, we use the attention score from layer 15 (index starting from 1) to choose the top-5 most attended image tokens as the candidate HITs.

B.3 Better OH Mitigation via Iterative Hallucinatory Objects Detection

In EAZY, for each text object tokens, we take their top- K most attended image tokens and take the union of all such sets as the zero-out list for HO detection inference. However, we realize that if we detect the hallucinatory objects iteratively, EAZY can achieve better hallucination mitigation performance. Specifically, assuming we extracted n text object tokens from the initial generation, we may take each of such top- K image tokens to zero out and observe if the corresponding object disappears from the new response. In such a case, candidate HITs from different text object tokens do not interfere with each other, enabling more effective detection and mitigation of hallucinations. We denote this iterative detection variant as EAZY (iterative) and represent its performance comparison

with EAZY in Table 8. It can be observed that EAZY (iterative) generally improved the performance on CHAIR with MSCOCO dataset.

METHOD	LLAVA-1.5		SHIKRA		LLAVA-NEXT	
	CHAIR _S ↓	CHAIR _T ↓	CHAIR _S ↓	CHAIR _T ↓	CHAIR _S ↓	CHAIR _T ↓
EAZY	38.8	11.4	26.6	8.9	26.8	8.3
EAZY (ITERATIVE)	37.8	10.9	26.2	8.7	25.6	8.5

Table 8: **Evaluation Results with CHAIR between EAZY and EAZY (iterative).**

B.4 Additional Evaluation Result of OH Detection

We provide the OH detection evaluation result of LLaVA-Next and Shikra in this section.

As shown in Tables 9 and 10, applying the EAZY method to LLaVA-Next and Shikra for hallucinated object (HO) detection demonstrates that EAZY continues to achieve superior performance across the majority of key metrics. In particular, EAZY exhibits significant advantages in overall accuracy and the precision of hallucinated object detection. Compared to the best-performing baseline, EAZY improves accuracy by 7.65% and 12.98% on LLaVA-Next and Shikra, respectively, while achieving gains of 46.98% and 23.56% in PR(OH). This highlights its effectiveness in correctly identifying hallucinated objects.

On the other hand, we observe that EAZY’s performance in detecting real objects is less pronounced for both models. We attribute this to differences in how LLaVA-Next and Shikra process image-to-image token transformations compared to LLaVA-1.5. Specifically, Shikra maps 576 image patch embeddings into 256 image tokens through an MLP, which causes visual information to intertwine and interfere with one another. Consequently, zeroing out specific image tokens may introduce inaccuracies. For LLaVA-Next, the model employs the AnyRes technique to split and resize the original image, requiring the removal of more image tokens than LLaVA-1.5. This likely impacts the detection of real objects by reducing the amount of preserved visual information.

Nevertheless, EAZY consistently demonstrates strong performance in object hallucination (OH) detection across both LLaVA-Next and Shikra, achieving the highest F1 scores of 80.12% and 76.61%, respectively. This indicates its superior ability to balance precision and recall, making it the most effective method overall. Particularly, EAZY achieves the highest recall on both models (92.67% on LLaVA-Next and 84.92% on Shikra), significantly surpassing the baseline methods. This suggests that EAZY effectively minimizes false negatives, ensuring that a larger proportion of hallucinated objects are correctly identified.

Furthermore, EAZY achieves the highest AUC scores in both ROC and Precision-Recall (PR) curve evaluations as shown in Figure 9 and 10. On LLaVA-Next, EAZY attains an AUC of 0.7688 for ROC and 0.9423 for PR, while on Shikra, it achieves 0.6903 for ROC and 0.8863 for PR. These results highlight EAZY’s ability to maintain a favorable trade-off between precision and recall, reinforcing its robustness across different vision-language models.

METRIC	UT	IC	EAZY
ACC	49.05	64.29	71.94
PR(RO)	87.75	87.39	70.57
PR(OH)	24.68	30.51	77.49
RECALL	42.32	64.77	92.67
F1	57.10	74.40	80.12

Table 9: **OH Detection Results using LLaVA-Next on Hall-COCO.** PR(RO) represents the precision of real objects (positive instances), while PR(OH) represents the precision of object hallucination (negative instances). UT [Zhou et al., 2023] is the uncertainty detection method. IC [Jiang et al., 2024] is the internal confidence method.

METRIC	UT	IC	EAZY
ACC	49.59	56.03	69.01
PR(RO)	77.33	81.87	69.77
PR(OH)	43.41	34.79	66.97
RECALL	55.60	50.80	84.92
F1	30.45	62.69	76.61

Table 10: **OH Detection Results using Shikra on Hall-COCO.** PR(RO) represents the precision of real objects (positive instances), while PR(OH) represents the precision of object hallucination (negative instances). **UT** [Zhou et al., 2023] is the uncertainty detection method. **IC** [Jiang et al., 2024] is the internal confidence method.

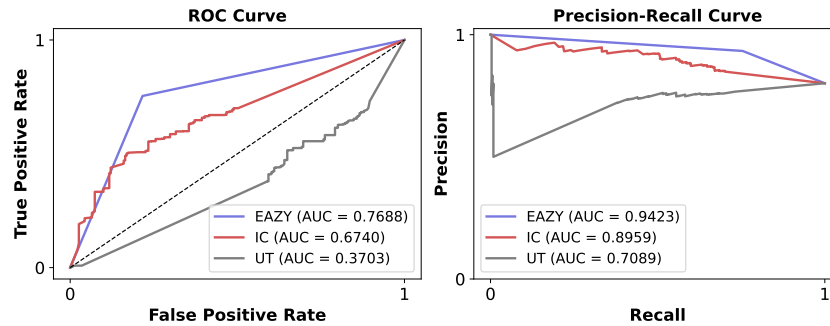


Figure 9: **Object Hallucination Detection Curves of LLaVA-Next on Hall-COCO.** We present the Precision-Recall and ROC curves of the proposed OH detection method and baselines.

C Efficiency Analysis

We evaluate the inference time (in seconds) on the LLaVA-1.5 7B under the CHAIR evaluation setting, which is close to the real-world application scenario. As shown in Figure 11, we present the average inference time over 500 image with the prompt "Please describe the image in detail.". We evaluate the different methods on NVIDIA A6000 GPUs. It can be observed the proposed EAZY method has 50% lower inference time than OPERA, while it brings significant performance improvement on object hallucination mitigation.

D Visual Bias is the Main Cause of Object Hallucination.

The causes of Object Hallucination (OH) are complex and may include factors such as training data, model architecture, cross-modal alignment, training paradigms, and inference methods. We focus on

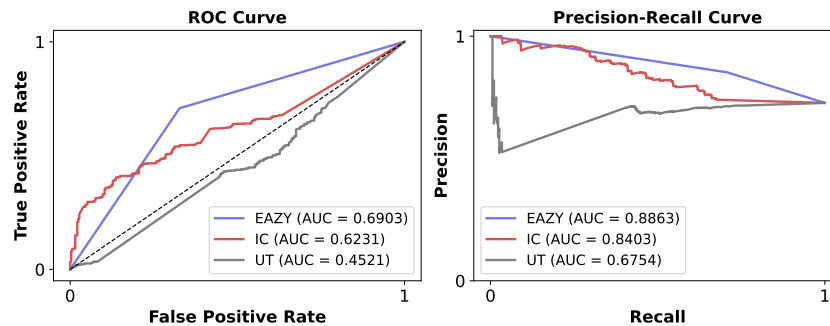


Figure 10: **Object Hallucination Detection Curves of Shikra on Hall-COCO.** We present the Precision-Recall and ROC curves of the proposed OH detection method and baselines.

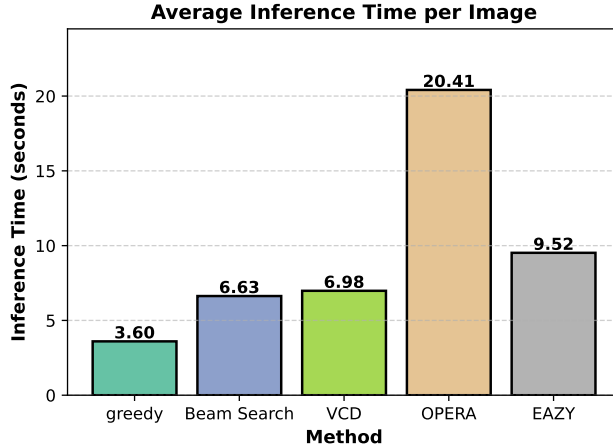


Figure 11: The average inference time of different methods on CHAIR evaluation.

factors that may lead to OH during the inference process, further exploring the impact of visual bias on OH and its proportion among different causes.

To simplify the problem, we categorize the factors causing OH during inference into three main categories:

- **Visual Bias**
 - Image Ambiguity: Low-resolution, misleading attributes (color, texture, shape), shadow, etc.
 - Modality Alignment: The gap between the mapped visual features and text features
- **Language Prior:**
 - Statistical learning bias of the language model leading to hallucination, including prior knowledge, grammar, co-occurrence, etc.
- **Others:**
 - Training Data Distribution Bias, Distribution imbalance hallucination, etc.

For a hallucinatory object, its emergence may result from multiple overlapping causes. If a specific factor is altered, causing the hallucinated object (HO) to disappear or change, we consider that factor to be the dominant cause of the HO.

Following with [Leng et al., 2024], we gradually add Gaussian noise on the image input to erase and weaken visual information. In such a case, we reduce the impact of visual bias while amplifying the influence of language priors and other factors. To evaluate the impact of visual bias in image inputs on object hallucination generation, we conducted experiments using LLaVA-1.5 on the Hall-COCO dataset. Specifically, we analyzed how the generation of hallucinated objects (HOs) changes when different levels of noise are added to the images. Specifically, we define New Hallucination as a newly generated hallucinatory object that appears after adding noise to the image. We define Stable Hallucination as a previously known hallucinatory object that persists even after applying noise. This suggests that Stable Hallucinations rely less on visual input and are instead more influenced by language priors.

As shown in Figure 12, we observe that as the noise time step increases, the image gradually becomes indistinguishable from pure Gaussian noise. First, we note that the number of hallucinatory objects gradually decreases. This is primarily due to the reduction in visual information, which leads the model to generate shorter text responses.

On the other hand, we find that the proportion of New Hallucinations significantly exceeds that of Stable Hallucinations, and the proportion of Stable Hallucinations continues to decline. After simply adding noise for 100 steps, the vast majority of hallucinatory objects are New Hallucinations, indicating that visual bias is a key factor driving the variation and generation of object hallucinations.

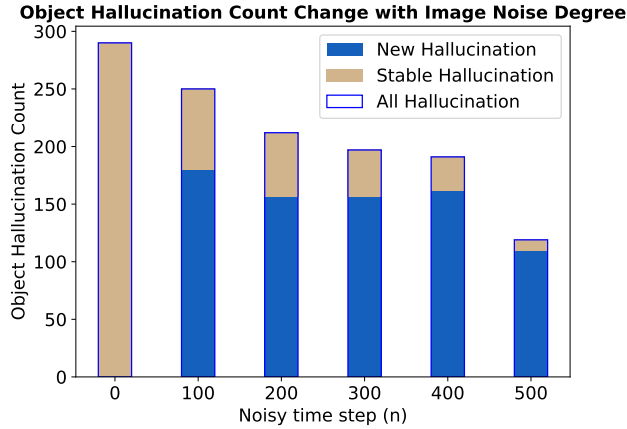


Figure 12: The amount change of different object hallucination along with the noise steps.

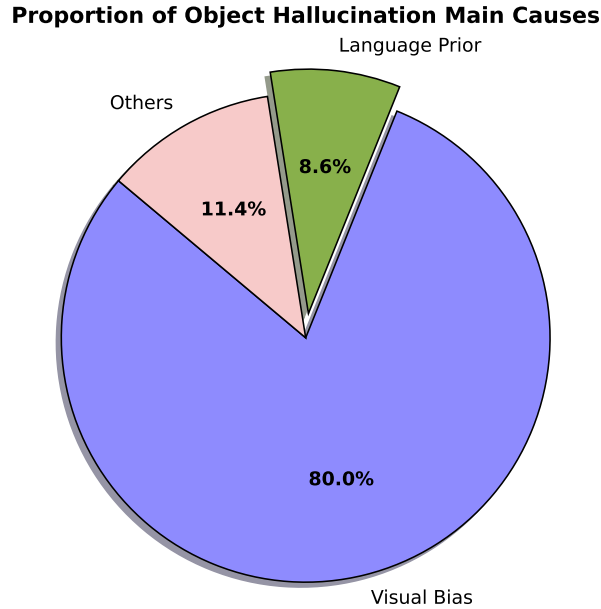


Figure 13: The proportion of different OH causes. Visual bias caused 80% of object hallucination changes.

To further estimate the relative impact of visual bias and language prior on object hallucination (OH), we fix the noise time step at 300. This setting largely removes visual information while avoiding excessive noise that would render the model’s output meaningless. We track the intersection of hallucinatory objects (HOs) that persist after applying EAZY on the original image and those that remain after adding 300-step Gaussian noise. Our findings indicate that 20% of all HOs are Stable Hallucinations, among which 43% cannot be eliminated by EAZY. As shown in Figure 13, this suggests that visual bias accounts for 80% of OH variations, while 8.6% of OHs are primarily influenced by language prior. The remaining 11.4% can be attributed to other factors.

E Hallucinatory objects are looking at image regions visually close to them.

In this section, we compare the attention score distribution of real objects and hallucinatory objects over image tokens. We visualize the text-to-image token-wise attention heatmap using the attention

from the 15th layer of the LLaVA-1.5 model. As shown in Figure 14, 16, 17 and 15, the attention distribution for real objects is typically concentrated on their corresponding image anchors. In contrast, hallucinatory objects follow two distinct attention patterns: (1) a dispersed attention distribution across different image regions, and (2) a highly concentrated focus on specific image regions that induce visual bias. Despite these differences, both patterns share a common characteristic—the attended regions often have some visual resemblance to the hallucinated object.

These regions often exhibit visual similarities to the hallucinated objects. For example, in Figure 14, the attention for *apple* is distributed over the *papaya* and *kiwi* regions—*papaya* shares a similar texture and color, while *kiwi* has a comparable shape. In Figure 15, the hallucinated object *television* primarily attends to the *microwave*, likely due to the visual resemblance of its glass panel and white frame to a television. In Figure 16, the hallucinated *baseball glove* directs all its attention to the baseball itself. Similarly, in Figure 17, the hallucinated *laptop* focuses on a black square notebook on the desk, which has a shape similar to a laptop.

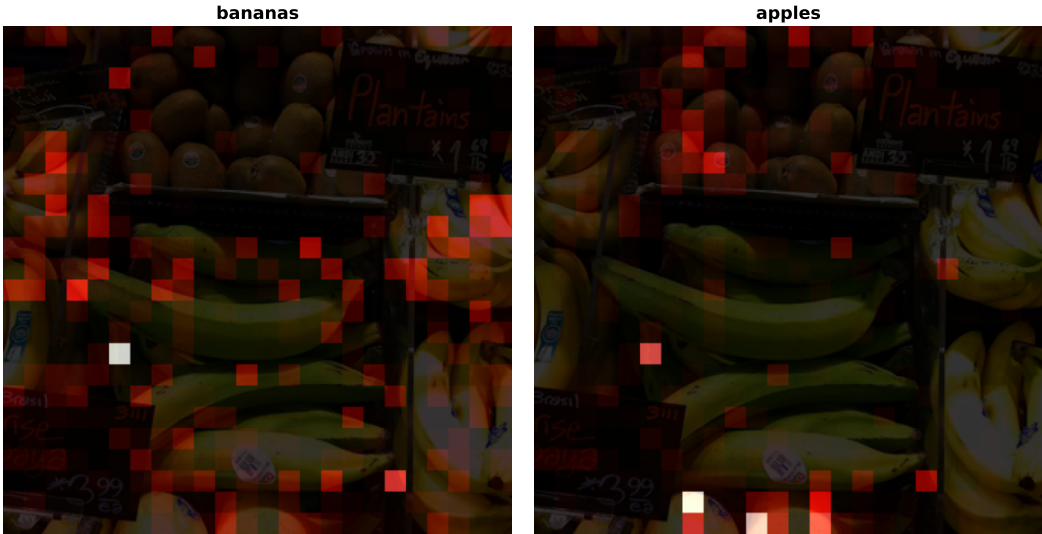


Figure 14: **Left:** The attention heatmap of the real object “*bananas*”; **Right:** The attention heatmap of the hallucinatory object “*apples*”.

F Failure Case Analysis.

We identify two typical cases of real objects being removed after applying EAZY. As shown in Figure 18, the small-size objects have the chance to be entirely removed from the image input, causing the model unable to recognize the objects. When the objects are located at the edge of the image with only part of them revealed, additionally, longer words are tokenized into multiple tokens, it may lead to the excessive removal of image tokens. Such an example can be seen in Figure 19.

G Discussion and Future Work

G.1 Summary of Key Findings

Our work provides a new perspective on understanding the causes and mechanisms of object hallucination in LVLMs—visual bias. We first demonstrate that LVLMs identify and extract object-related information from image tokens in their early-middle to late-middle layers. This finding leads us to an important and intriguing phenomenon-Hallucinatory Image Tokens (HITs). By removing only a small subset of these tokens, we can significantly mitigate object hallucination in LVLm-generated outputs.

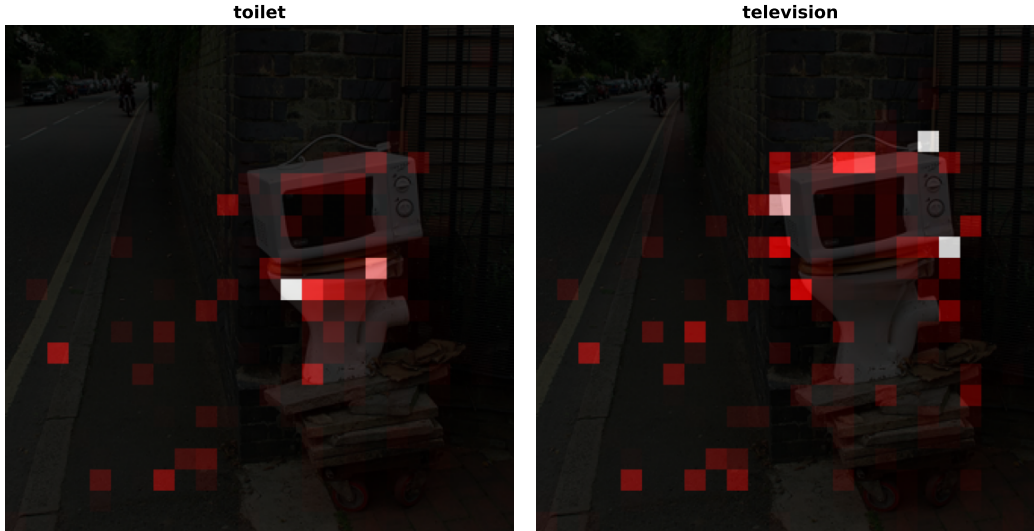


Figure 15: **Left:** The attention heatmap of the real object“*toilet*”; **Right:** The attention heatmap of the hallucinatory object“*television*”.

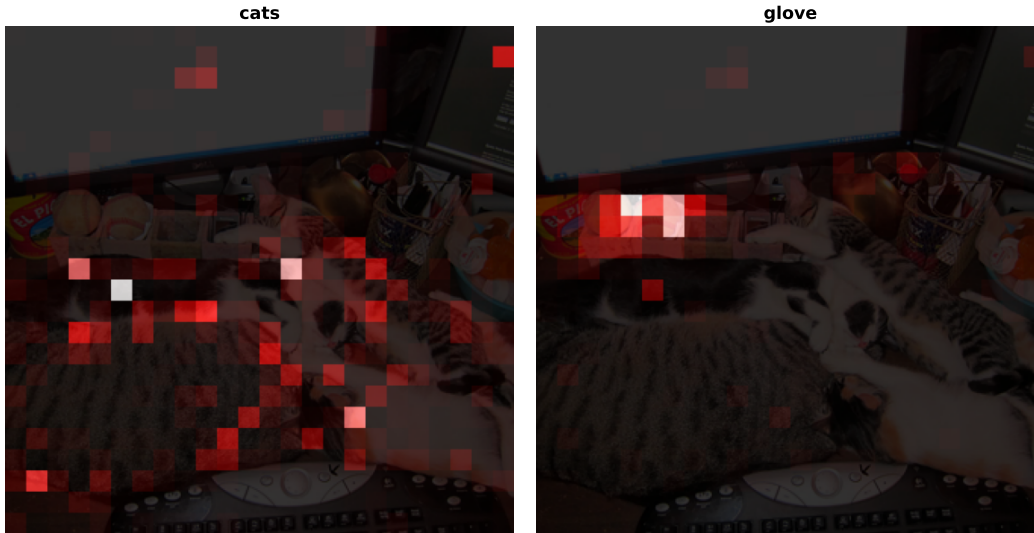


Figure 16: **Left:** The attention heatmap of the real object“*cats*”; **Right:** The attention heatmap of the hallucinatory object“*glove*”.

Building on this discovery, we propose EAZY, a training-free approach that effectively detects and mitigates OH. By replacing the top- K candidate HITs with zero embeddings, EAZY successfully suppresses hallucinated objects while preserving real object information. Our experiments demonstrated the superior performance of EAZY on HO detection and mitigation.

G.2 Limitations and Future Work

Our work leads to two promising questions. The first is achieving a deeper understanding of the HITs phenomenon. We found that existing interpretability tools, such as the Logit Lens, are insufficient for fully explaining and identifying all HITs. In future work, we aim to gain a more comprehensive understanding of HITs and leverage advanced interpretability tools to better distinguish them from

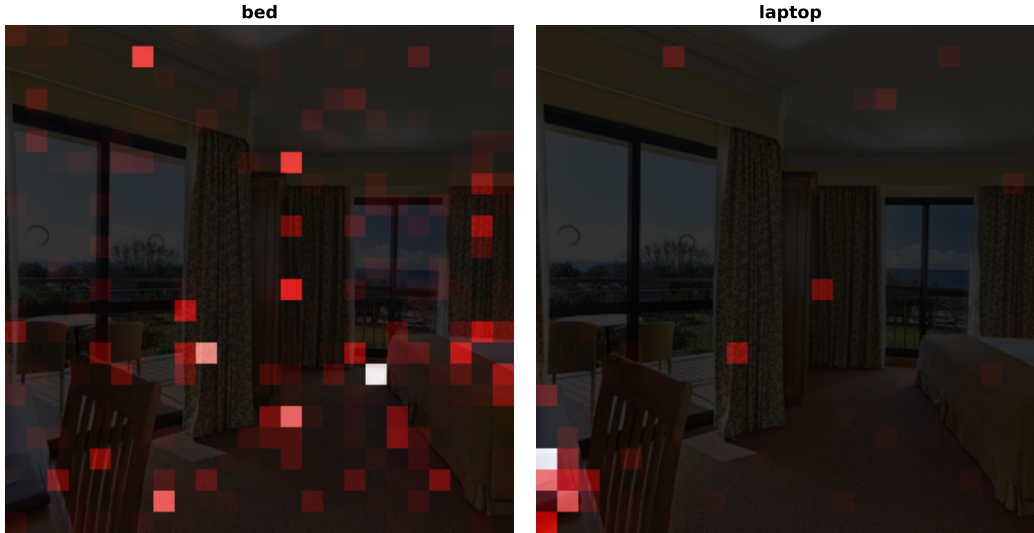


Figure 17: **Left:** The attention heatmap of the real object “*bed*”; **Right:** The attention heatmap of the hallucinatory object “*laptop*”.

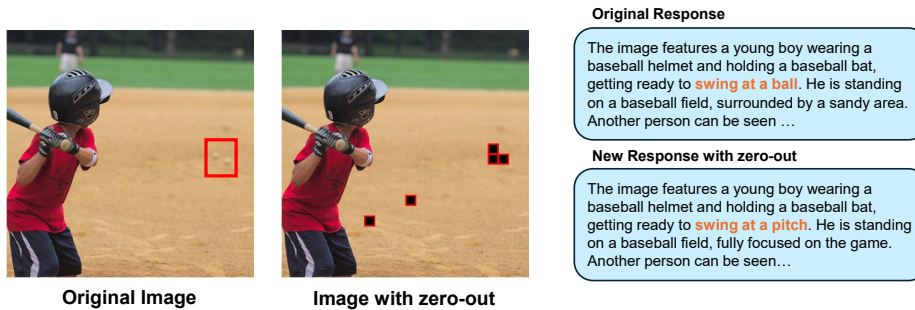


Figure 18: **Failure case of object “ball”.** The original response successfully recognizes the “ball” on the ground. Due to the small size, applying zero-out directly masks the ball object from the image, resulting in the disappearance of the “ball” in the new response

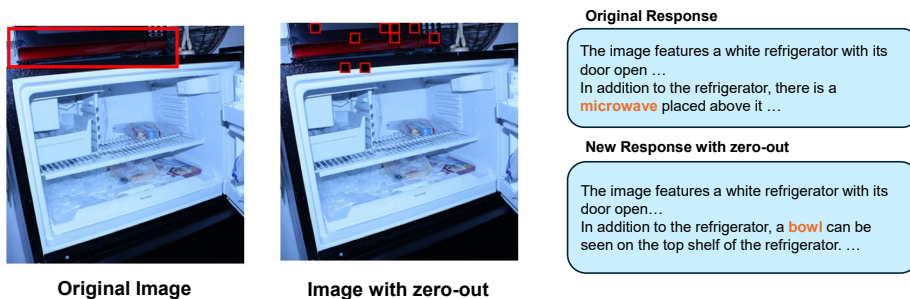


Figure 19: **Failure case of object “microwave”.** The word “microwave” is split into “mic”, “row” and “ave”, which significantly increase the number of image tokens for zeroing out. In addition, this object is located on the edge of the image, with only part of it shown in the image. The new response does not have the “microwave” in it.

their top- K candidates, thereby significantly improving the efficiency of EAZY in zeroing out image tokens.

The second lies in EAZY’s handling of real objects. As discussed in Appendix F, EAZY may occasionally misclassify real objects—particularly those that are small in size, tokenized into multiple tokens, or located at the image boundaries—and erroneously remove them from the generated response. To address this, we plan to explore the following directions:

1. Performing multiple inferences to assess the robustness of different object tokens.
2. Incorporating additional features, such as uncertainty estimation, to improve the detection accuracy.
3. Integrating external vision models to refine object identification and mitigate errors.

We hope that the findings of this work will contribute to a deeper understanding of object hallucination in LVLMs, inspire future research, and enable broader applications of the HITs phenomenon in vision-language models.

H Case Study

Please refer to the next page for more visualization cases.

Please describe the image in detail.

User

Regular Decoding

LLaVA-1.5

The image features a large airport tarmac with several airport workers and vehicles. There are two men on a small cart, pulling a large cargo container, possibly a shipping container or a piece of luggage. Another man is standing nearby, possibly observing the process or waiting for his turn to assist.

In addition to the workers and the cart, there are two **motorcycles** on the tarmac, one located closer to the left side and the other towards the right side of the scene. A **truck** can also be seen in the background, likely used for transporting cargo or luggage. The overall scene depicts a busy airport environment with workers handling various tasks.

EAZY

LLaVA-1.5

The image features a man driving a small vehicle, possibly a golf cart, pulling a large cargo container on the tarmac. The man is wearing a **white helmet** and appears to be in the process of loading or unloading the cargo. Another person is standing nearby, possibly assisting with the task.

In the background, there is an **airplane** visible, indicating that the scene takes place at an airport. The **cargo container** is quite large, occupying a significant portion of the tarmac area. The presence of the airplane and the cargo container suggests that the airport is actively handling **cargo transportation and logistics**.

Figure 20: **Case 1:** When using original greedy decoding, the response generated by LLaVA-1.5 model contains "motorcycles" and "truck", two HOs. After using EAZY to remove five image tokens, it can be observed the HOs disappeared in the new response with more details and better description.

Please describe the image in detail.

User

Regular Decoding

LLaVA-1.5

The image features a window with a potted plant placed on a window sill. The plant is positioned in the middle of the window, and it appears to be a vase with flowers. The window is adorned with a yellow curtain, which adds a touch of color to the scene.

In the background, there is a **person** partially visible, standing near the window. The scene appears to be set in a room with a brick wall, giving it a cozy and warm atmosphere.

EAZY

LLaVA-1.5

The image features a window with a potted plant placed on a window sill. The plant is positioned in the middle of the window, and it appears to be a vase with flowers. The window is adorned with a yellow curtain, which adds a touch of color to the scene.

In the background, there is a **building** visible, possibly a neighboring structure or a part of the same building. The combination of the window, potted plant, and the yellow curtain creates a cozy and inviting atmosphere.

Figure 21: **Case 2:** The LLaVA-1.5 falsely recognized a nonexistent person in the image. EAZY identified the building reflected in the window.

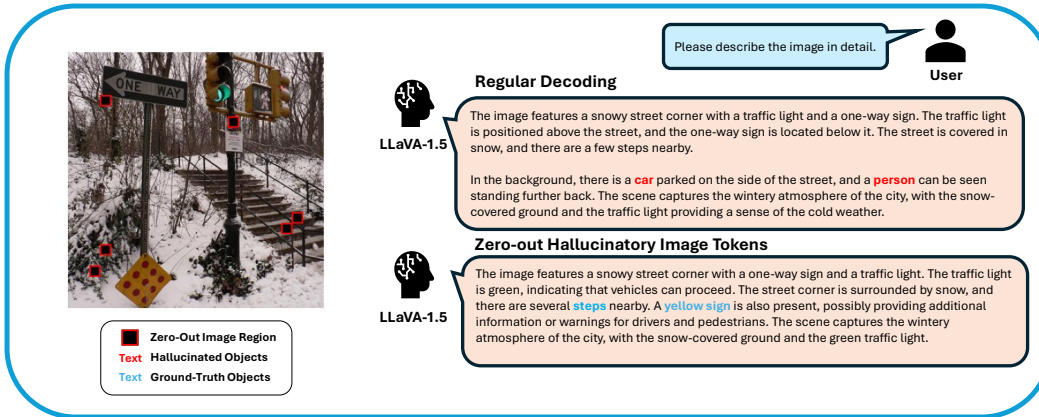


Figure 22: **Case 3:** In the original response, the model identified a car and a person in the image. EAZY successfully helped the model recognize the steps and the yellow markings while eliminating the previous hallucinations.

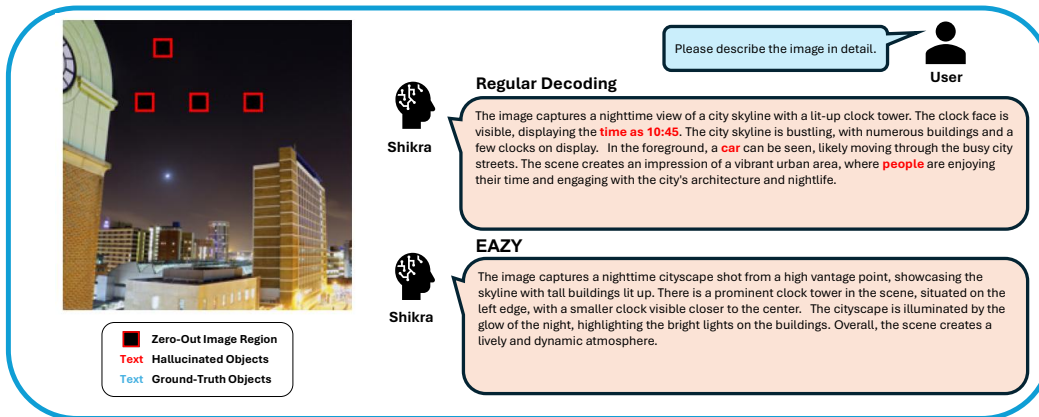


Figure 23: **Case 4:** EAZY not only removed the hallucinated objects (*car* and *people*) but also corrected the inaccurate clock time.

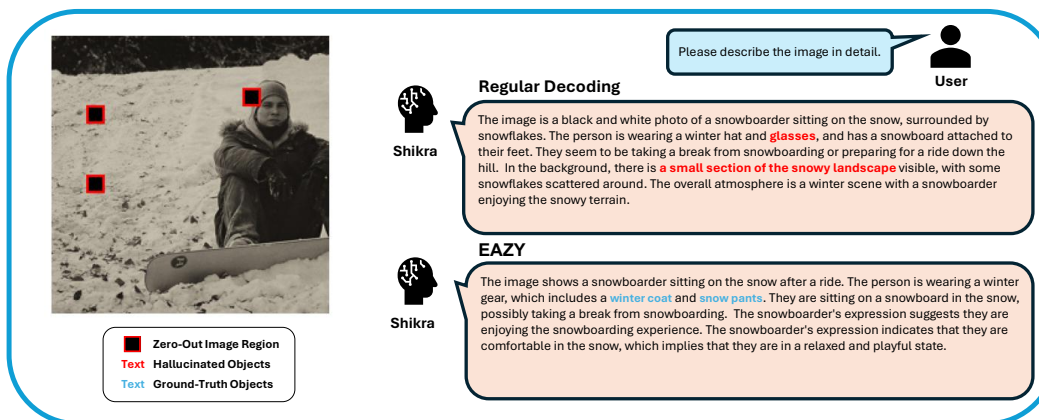
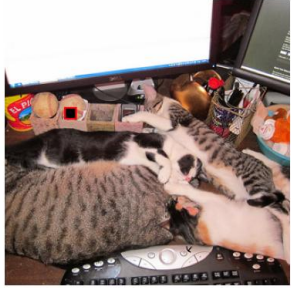


Figure 24: **Case 5:** EAZY corrected the hallucinated object (*glasses*) and adjusted the inaccurate description of the background environment (*a small section of the snowy landscape*).



■ Zero-Out Image Region
Text Hallucinated Objects
Text Ground-Truth Objects

Please describe the image in detail.

User

Regular Decoding

The image features a wooden desk with a computer monitor and keyboard on it. A group of cats is lying down on the desk, with some of them sleeping and others playing. There are a total of **five cats** in the scene, with one cat lying on the left side of the desk, another on the right side, and three cats in the middle.


In addition to the cats, there are several objects on the desk. A **baseball glove** is placed near the left side of the desk, and a bottle can be seen on the right side. There are also **two cups**, one near the center of the desk and the other closer to the right side. A bowl is located on the right side of the desk, and a **cell phone** is placed near the center.

EAZY

The image features a wooden desk with a computer keyboard and a computer monitor. On the desk, there are **four cats** lying down, seemingly sleeping or relaxing. The cats are spread out across the desk, with one cat on the left side, another in the middle, and two more on the right side.

In addition to the cats, there are several objects on the desk. A **baseball** is located near the left side of the desk, while a bottle can be seen on the right side. A **cup** is also present on the right side of the desk, and a bowl is placed near the center.

Figure 25: **Case 6:** By zeroing out just a single image token, the model successfully identified the correct number of cats and cups in the image while removing the hallucinated objects *baseball glove* and *cell phone*.



■ Zero-Out Image Region
Text Hallucinated Objects
Text Ground-Truth Objects

Please describe the image in detail.

User

Regular Decoding

The image features a unique clock statue located in an open area, possibly a city park or plaza. The clock is situated on top of a podium, with its large clock face facing the viewer. Two eagle statues are positioned on either side of the clock, adding an interesting artistic touch to the area. Additionally, there are **two cars** parked in the background, near the edge of the open area. A **person** can also be seen in the middle of the scene, possibly admiring the clock and eagle statues.

EAZY

The image features a large clock on top of a building, with two tall birds on either side of it. The clock is situated in the middle of the scene, drawing attention to the time it displays. The sky serves as a background for the clock and the birds, creating a unique and interesting atmosphere. Additionally, there is a **car** parked in the background on the left side of the scene. The presence of the car indicates that this area might be a public space or a place with some degree of human activity.

Figure 26: **Case 7:** With EAZY, the number of cars in the new response was correctly identified, and the hallucinated object *person* was successfully removed.